



Attivissimo, F., Di Nisio, A., Lanzolla, A. M. L., and Paul, M. (2015) Feasibility of a photovoltaic-thermoelectric generator: performance analysis and simulation results. IEEE Transactions on Instrumentation and Measurement,

Copyright © 2015 IEEE

A copy can be downloaded for personal non-commercial research or study, without prior permission or charge

Content must not be changed in any way or reproduced in any format or medium without the formal permission of the copyright holder(s)

When referring to this work, full bibliographic details must be given

<http://eprints.gla.ac.uk/104566>

Deposited on: 31 March 2015

Enlighten – Research publications by members of the University of Glasgow_
<http://eprints.gla.ac.uk>

1 Feasibility of a Photovoltaic-thermoelectric generator: Performance Analysis and 2 Simulation Results

3 *F. Attivissimo*¹, *IEEE Member*, *A. Di Nisio*¹, *IEEE Member*, *A. M. L. Lanzolla*¹, *IEEE Member* and *M. Paul*²

4 ¹Department of Electrical and Information Engineering (DEI)

5 Polytechnic of Bari

6 Via E. Orabona 4, 70125 Bari Italy

7 [attivissimo, dinisio, lanzolla]@misura.poliba.it

8 ²School of Engineering, University of Glasgow,

9 Glasgow G12 8QQ, UK

10 Manosh.Paul@glasgow.ac.uk

11
12
13 **Abstract** – The paper describes a theoretical approach to evaluate the performance of a
14 hybrid solar system made with photovoltaic cells and thermoelectric modules. After a brief
15 treatment of the integrated system, energy conversion and performance parameters are
16 evaluated through numerical simulations depending on the global radiation and temperature
17 distribution obtained by the Joint Research Centre of the European Commission and of the
18 National Renewable Energy Laboratory. The contributes of thermoelectric module to total
19 energy seems significant in southern Europe towns and less substantial when the locations
20 considered are very distant from the equator and show the possibility of using thermoelectric
21 devices for energy production.
22

23 **Keywords** – *Solar cells, photovoltaic solar energy, photovoltaic cell model, thermoelectric*
24 *conversion, thermoelectric module model, conversion efficiency.*

25 TERMINOLOGY

26	α	temperature coefficient for short-circuit current [A/K]
27	A_p	photovoltaic module surface [m ²]
28	A_t	thermo-element area [mm ²]
29	E_g	energy band gap [eV]
30	ε_{STC}	efficiency at Standard Test Conditions (STC)
31	ε	efficiency
32	ε_{PVTE}	efficiency of photovoltaic- thermoelectric module
33	ε_{TE}	efficiency of thermoelectric module ε_{PV} efficiency of photovoltaic module
34	FF	fill factor

35	G_{ref}	irradiance at STC [W/m^2]
36	G	irradiance on horizontal surface [W/m^2]
37	I	thermo-module current [A]
38	I_L	photo-generated current [A]
39	I_{OD1}, I_{OD2}	reverse saturation diode current [A]
40	I_{sc}	short-circuit current in STC [A]
41	I_{mp}	current at maximum power point [A]
42	k	Boltzmann's constant [J/K]
43	h_t	thermo-element length [mm]
44	h_c	copper contact length [mm]
45	h_p	ceramic element length [mm]
46	h_s	ratio between contact superficial electric resistivity and the thermo-element electric resistivity [mm]
47	A_t	thermo-element area [mm^2]
48	n_1, n_2	ideality factor
49	s	thermocouple Seebeck coefficient [V/K]
50	λ	thermocouple thermal conductivity [W/mm K]
51	ρ	thermocouple electric resistivity [Ω mm]
52	ρ_c	contact superficial resistivity [Ω mm^2]
53	λ_p	ceramic isolator thermal conductivity [W/mm K]
54	P_n	nominal power of the photovoltaic of the solar generator [W]
55	$P_{out_{PV}}$	electrical power output of the PV module [W]
56	$P_{out_{TE}}$	electrical power output of the TE module [W]
57	$P_{out_{PVTE}}$	electrical power output of the PV/TE system [W]
58	Q	rate of heat liberated by the thermoelectric module [W]
59	Q_{TE}	rate of heat liberated by the thermocouple [W]
60	R_{in}	thermo-module resistance [Ω]
61	R_L	electric load resistance [Ω]
62	R_S	series resistance [Ω]
63	R_{Sh}	shunt resistance [Ω]
64	T_{ref}	cell temperature at STC [K]
65	T_{max}	maximum photovoltaic module temperature [K]
66	T_{amb}	ambient temperature [K]
67	T_m	operating temperature [K]
68	T_{avg}	average temperature [K]
69	T'_h	hot junction temperature [K]
70	T'_c	cold junction temperature [K]
71	T	cell temperature [K]
72	V	voltage [V]
73	V_o	thermoelectric generator open-circuit voltage [V]

74	V_{oc}	open-circuit voltage in STC [V]
75	V_T	thermal voltage [V]
76	V_{mp}	voltage at maximum power point [V]

77
78

79 I. INTRODUCTION

80 In recent years, the fast development and the growing demand of comfort is rising the
81 energy consumption; surging oil and gas consumption and increasing environmental
82 awareness has prompted more and more sustainable development [1]; originally born as a
83 problem of ethics and morality, the development of the alternative energy sources became a
84 pressing requirement since the global pollution problem has become relevant. In the last
85 decade, photovoltaic (PV) technology has attracted strong interest of the industry and of many
86 researchers [2]. Research on solar cell was made since 1960 and different technologies have
87 been proposed in order to reduce the material and to increase the production capacity.

88 At present silicon modules represent the leading PV technology thanks to both their
89 capability to provide high efficiency and the great availability of silicon material on the earth.
90 In particular monocrystalline solar cells offer highest efficiency with more than 20% [3]. Two
91 alternative typologies developed to reduce the cost in PV modules production are (i) the
92 polycrystalline silicon which provides worse performance in terms of efficiency (13-16%) and
93 (ii) the amorphous silicon which offer low efficiency (6-9%) but is less affected by high
94 temperatures and shading.

95 With respect to the PV cells based on crystalline silicon, thin film technology is less
96 expensive since it uses few materials and less manufacturing process. Depending on the
97 technology, thin-film module prototypes have reached efficiencies between 7–13% [4], [5].

98 Despite PV is considered a commercially mature technology, the efficiency of the PV
99 plants is still quite low, therefore in the best of cases about 80% of the potential energy
100 available would be wasted. On the other hand, this technology reduces continuously its cost
101 and requires technical advance and new research for efficiency increment [6], [7]. Therefore,
102 many researches have focused on the reduction of the losses that affect solar panels such as
103 losses caused by the sunlight, the conditioning circuit required, the energy storage system, the
104 Joule effect and so on [8], [9].

105 In order to reduce these effects, researchers are focusing on two strategies: to develop new
106 materials or to try recovering part of the energy lost as heat by Joule effect [10], [11].
107 Therefore, nowadays, panel's manufacturers have high interest in combining thermoelectric

108 (TE) and photovoltaic effects to obtain higher performance. The low efficiency of TE energy
109 conversion has limited the use of TE in electric power generation but this technology is
110 evolving to a higher level of performance [12]. On the other hand, TE generators are preferred
111 to recovery large amounts of waste heat or when the thermal input is free. Common
112 applications of this conversion are the energy recovery from the waste heat of electronic hot
113 components or cooling and heating PV elements in order to increase its efficiency or
114 powering autonomous sensors [13]-[16]. Latest applications of the TE conversion are
115 addressed to PV systems as active cooling or additional power generation of PV panels both
116 using the difference between the ambient temperature and high panel temperature caused by
117 the solar irradiation. The performance of a TE module is represented by the so-called figure of
118 merit (Z) of the TE material or by the dimensionless ZT_{avg} product [23], [24], being T_{avg} the
119 average temperature of the TE module.

120 The figure of merit Z represents the conversion efficiency from thermal energy into
121 electrical energy and is strongly TE materials dependent. To optimize this parameter a large
122 Seebeck coefficient, high electrical conductivity and low thermal conductivity are required.

123 For near room temperature applications (300 K) bismuth chalcogenides such as Bi_2Te_3 or
124 Bi_2Se_3 materials provides the greatest figure of merit; for mid temperatures (500-900 K)
125 Magnesium group IV compounds are mainly preferred; instead for high temperatures silicon –
126 germanium materials are typically used.

127 Typical values of ZT_{avg} range in [0.7-0.8] but materials currently available reach values of
128 1; ZT_{avg} goes beyond of 1.2 for nanostructured bismuth antimony telluride bulk alloys [25]. In
129 TABLE I. standard values of figure of merit are listed for different thermoelectric materials.

130 A hybrid photovoltaic-thermoelectric (PVTE) system can be found in many configurations
131 where the two modules can be separated or integrated. No integrated hybrid systems are
132 retrievable in cars [27], in some systems of harvesting energy, in particular types of
133 telecommunication applications [28]; in some cases, these two modules are separated
134 requiring an electronic controller [29], [30]. The integrated panels combine these devices in
135 order to optimize the performance of both sources [9]. In this paper the performances of an
136 integrated PVTE system was analyzed varying the site and using solar irradiation, temperature
137 and sunshine hours available on solar energy database of the European Joint Research Centre
138 [31]. Using databases of irradiance, temperature and other climatic parameters the authors
139 evaluate the annual performance of the PVTE system at different European sites analyzing the
140 additional TE power; the consistency of data used, with a ten years coverage over most of the

141 regions considered, assure the reliability of the obtained results and can provide information
 142 to investors, authorities and renewable energy market.

143 For this aim, first the theory of PV and TE conversion is shortly summarized; then the
 144 model and the estimation algorithms of both photovoltaic and thermoelectric modules are
 145 implemented with Matlab functions and verified by simulating commercial modules.

146 **TABLE I.** FIGURE OF MERIT FOR DIFFERENT THERMOELECTRIC MATERIALS [26]

Thermoelectric material	Material name	Manufacturing type	ZT_{avg}	Scenario Temperature
Chalcogenides	Bi_2Te_3	bulk	0.74	low
	$\text{Bi}_{0.52}\text{Sb}_{1.48}\text{Te}_3$	bulk	1.05	low
	$\text{Bi}_{0.52}\text{Sb}_{1.48}\text{Te}_3$	nanobulk	0.52	low
	$\text{Na}_{0.0283}\text{Pb}_{0.945}\text{Te}_{0.9733}$	nanobulk	1.45	high
Silicon-germanium	SiGe	bulk	0.3	high
	$\text{Si}_{80}\text{Ge}_{20}$	banowire	0.53	high
	SiGe	nanobulk	0.22	low
Skutterudites	$\text{CeFe}_4\text{Sb}_{12}$	bulk	0.77	high
	$\text{Yb}_{0.2}\text{In}_{0.2}\text{Co}_4\text{Sb}_{12}$	bulk	0.93	high
	$\text{Ca}_{0.18}\text{Co}_{3.97}\text{Ni}_{0.03}\text{Sb}_{12.40}$	bulk	0.77	high
Oxides	$\text{Ca}_{2.4}\text{Bi}_{0.3}\text{Na}_{0.3}\text{Co}_4\text{O}_9$	bulk	0.13	high

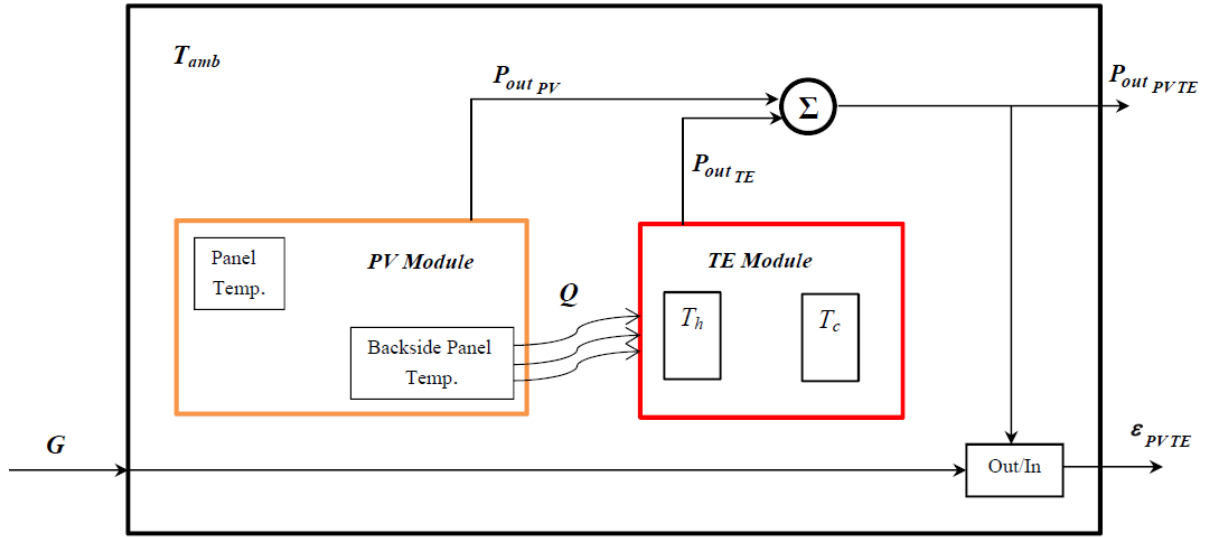
147

148

149 II. THE MODEL

150 A. SYSTEM LAYOUT AND ASSUMPTIONS

151 A schematic representation of the PVTE system is reported in Fig.1 where the two blocks
 152 represent the PV and the TE modules; the thermal energy generated in the first block is
 153 converted to electricity by the second block. These elements can be reasonably considered
 154 separately, since the effects that lead to the generation of current can be considered
 155 independent of each other; indeed, even if the TE module is posteriorly integrated into the
 156 solar panel, and it exploits the temperature of the rear of the panel itself, this phenomenon
 157 affects the solar cell performance in a reasonably negligible way.



158

159

Fig.1 - PVTE hybrid system representation

160 The system operates at room temperature having as input the solar radiation and as output the
 161 total electric power generated by the system. At high solar irradiance the PV module
 162 temperature (T_{max}) can reach 50-60 °C and differs from room temperature by about 30°- 40° C
 163 (ΔT). These values depend on the site, the type of the integration and of the period of year
 164 considered. To calculate the PV panel temperature (T), which strongly depends on the
 165 incident light, the working conditions and the installation conditions, the following relation
 166 was used [32]:

$$167 \quad T = T_{amb} + c \cdot G \quad (1)$$

168 being G [W/m^2] the irradiance and c [$\text{K} \cdot \text{m}^2/\text{W}$] a coefficient, known as the Ross coefficient,
 169 which depends on the installation conditions of the PV panel. The values of c are $0.058 \text{ K} \cdot$
 170 m^2/W for roof PV panels integrated, $0.036 \text{ K} \cdot \text{m}^2/\text{W}$ for top of roof with small roof-module
 171 distance ($<10 \text{ cm}$), $0.027 \text{ K} \cdot \text{m}^2/\text{W}$ for on top of roof with large roof-module distance ($>$
 172 10cm), and $0.020 \text{ K} \cdot \text{m}^2/\text{W}$ for free-standing.

173 In TABLE II. the obtained values for the six considered sites [31] are listed, where T_{max}
 174 represents the maximum value of the panel temperature and ΔT is the difference between
 175 T_{max} and T_{amb} at different c for each town considered.

176

177

179 **TABLE II.** MAX VALUES OF MODULE TEMPERATURE AND TEMPERATURE DIFFERENCE AT DIFFERENT
 180 SITES FOR DIFFERENT PV INSTALLATION CONDITIONS

City	T_{max} [°C]				ΔT [°C]			
	c=0.058	c =0.036	c =0.027	c =0.020	c=0.058	c =0.036	c =0.027	c =0.020
	K·m ² /W	K·m ² /W	K·m ² /W	K·m ² /W	K·m ² /W	K·m ² /W	K·m ² /W	K·m ² /W
Pachino (Sicily)	60	48	43	39	32	20	15	11
Taranto	58	46	41	38	31	19	14	11
Rome	56	45	40	36	30	19	14	10
Turin	50	41	37	34	26	16	12	9
Glasgow	32	26	23	22	16	10	7	5
Stockholm	37	30	28	25	18	11	8	6

181

182 The performance of the combined system should be given in terms of both generated electric
 183 power and overall system efficiency by highlighting their dependence on environmental
 184 conditions, such as temperature and radiation, and on physical properties of the used material.

185 Starting from these considerations the principle of superposition is therefore usable; then
 186 the generated electrical power of the overall system will be the sum of the electric powers
 187 generated by both modules. Under this assumption the overall efficiency of the system can be
 188 calculated as the ratio between the sum of the generated electric powers by each module, and
 189 the power of the input system, i.e. the solar radiation available to the PV module. In this case,
 190 both the front face temperature (T) and operating temperature of TE (T_m) will determine the
 191 PV and the TE module performance, respectively. Precisely, the temperature of the cells
 192 within the PV module (T) will depend on the ambient temperature (T_{amb}) and on the incident
 193 solar radiation flux (G); the operating TE temperature (T_m) will depend on rear panel
 194 temperature (T_h) and on the ambient temperature (T_{amb}). It is useful to note that there is a heat
 195 flow (Q) going from the PV to the TE module which is dissipated through the latter. Finally,
 196 in order to preserve the energy balance, the following losses should be considered:

- 197 • transformation losses due to conditioning circuits of the PV module (there are in fact
 198 inverter and other circuitries), which are not included in the model;
- 199 • losses due to the Joule effect in the PV module;
- 200 • losses due to the Joule effect in the TE module;
- 201 • losses due to dispersion currents;
- 202 • convection losses.

203 .

204 B. PV MATHEMATICAL MODEL

205 The simplest equivalent circuit of a PV cell consists of p-n junctions with a current
206 generator current having intensity dependent on the incident radiation power:

$$207 \quad I_L(T, G) = I_{SC}(T_{ref}, G_{ref}) \frac{G}{G_{ref}} [1 + \alpha(T - T_{ref})] \quad (2)$$

208 where the parameter T points out the influence of the temperature on the solar cell. Both
209 simulation and characterization of PV cells require parametric estimation of the model's
210 parameters and many works are dedicated to this issue [33]; in [34] and an equivalent circuit
211 with its parameters evaluation is presented, whereas in [35] an equivalent circuit based on
212 double-diode representation is used. The mathematical model uses a current source having
213 intensity proportional to the incident radiance and two diodes simulating diffusion and
214 recombination processes. This accurate model highlights different physical characteristics
215 which are independent from each other:

$$216 \quad I = I_L - I_{0D1} \left[e^{\frac{(V+R_s \cdot I)}{V_T \cdot n_1}} - 1 \right] - I_{0D2} \left[e^{\frac{(V+R_s \cdot I)}{V_T \cdot n_2}} - 1 \right] - \frac{V + R_s \cdot I}{R_{Sh}} \quad (3)$$

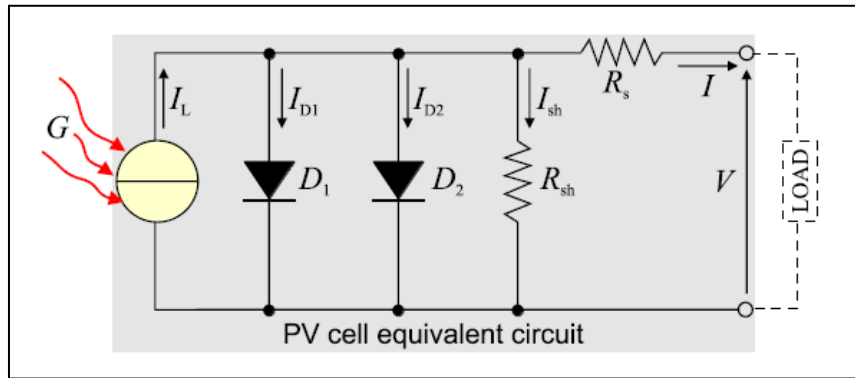
217 where:

- 218 • $V_T = k \cdot T / q$
- 219 • q is the electron charge ($1.602 \cdot 10^{-19}$ C) and k the Boltzmann's constant ($1.38 \cdot 10^{-23}$ J/K);
- 220 • T is the absolute temperature (K) of the p-n junction
- 221 • I_{0D1} and I_{0D2} are the reverse saturation currents of the two diodes;
- 222 • n_1 and n_2 are the diodes ideality factors;
- 223 • R_s is the equivalent series resistance of the cell and R_{Sh} is the equivalent shunt resistance.

224

225 The saturation currents in model (3) depend on the intrinsic characteristics of the PV cell,
226 which in turn depend on several physical parameters that are not usually available for the
227 commercial PV arrays. The diode ideality factors values may be arbitrarily chosen but
228 generally the initial values $n_1=1$ and $n_2=2$ can be selected in order to identify the model. A
229 right estimation of these six parameters would be obtained by best fitting the model with a
230 real panel. In Fig.2 the first diode represents the recombination current in the almost-neutral
231 regions, while the second one represents recombination in the depletion region. In the same
232 figure, R_s is the series resistance including the silicon wafer, the contact resistance and, also,

233 the circuital resistance derived from connections to the terminals and thus, materially,
 234 represents losses by Joule effect. R_{sh} is the parallel resistance deriving from leakage currents
 235 at the solar cell edges and from the inhomogeneity of the surface's; it represents the losses due
 236 to leakage current towards ground. Both resistors make the characteristic curve less
 237 "rectangularly shaped" and they reduce the maximum output power. In an ideal solar cell,
 238 obviously the resistance values of R_s and R_{sh} should theoretically be zero and infinity
 239 respectively an assumption often used in the analysis and characterization of the panels.
 240



241
 242 Fig.2 - Two diodes equivalent circuit of a PV cell

243 The extension of the model to a PV panel and a parallel string produces the equations [36]:

$$\begin{aligned}
 I_{\text{module}} &= N_p \cdot I; V_{\text{module}} = N_s \cdot V \\
 R_{s \text{ module}} &= R_s \cdot N_s / N_p; R_{sh \text{ module}} = R_{sh} \cdot N_s / N_p
 \end{aligned}
 \tag{4}$$

245 where a string is made of N_s cells in series, and a module is composed by N_p strings in parallel
 246 with the hypothesis that all the cells are identical and are subjected to the same radiance and
 247 temperature. This kind of model, known in the literature as *seven-parameters model* (I_L , I_{OD1} ,
 248 I_{OD2} , n_1 , n_2 , R_s , R_{sh}), was already analysed by the authors using the Newton-Raphson method
 249 and its applicability to different plants has been verified [37].
 250

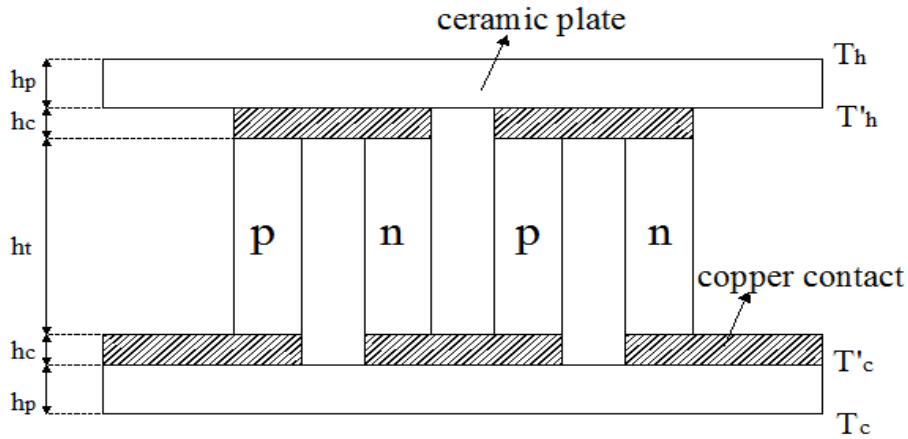
251 C. TE MATHEMATICAL MODEL AND ITS VERIFICATION

252 The fundamental element of a TE module is the thermocouple which is realized with two
 253 legs of a different doped semiconductor material; they are made of n-type and p-type doped
 254 semiconductor doped and are connected to each other by a metal plate usually made of
 255 copper.

256 In Fig.3 a generic TE module with N_{TE} thermocouples connected electrically in series and
 257 thermally in parallel is represented where h_p is the ceramic plate length, h_t and A_t are the
 258 length and the cross-sectional area of the thermo-elements and h_c represents the copper
 259 contact length.

260

261



262

263

Fig.3 – Basic structure of a TE module

264 The thermal power extracted by a TE module is the result of the Peltier, Joule and Fourier
 265 effects which model this phenomenon by means of the Seebeck coefficient s , the electrical
 266 resistivity ρ and the thermal conductance λ of the material and of thermo-elements geometry
 267 as function of both hot-side T_h and cold-side T_c temperatures [38]:

$$268 \quad Q_{TE} = N_{TE} \left[\lambda \frac{A_t}{h_t} (T_h - T_c) + s \cdot T_h \cdot I - \frac{1}{2} R \cdot I^2 \right] \quad (5)$$

269 being I the thermo-module current and $R = \rho \cdot h_t / A_t$. Equation (5) is a simplified model of a
 270 TE module which consists of two semiconductor thermo-elements connected by conducting
 271 copper strips. A more accurate and realistic model requires to consider the thermal and
 272 electrical contact resistances between the thermo-elements and the ceramic plates. Precisely,
 273 the effect associated with ceramic layers, reduces the effective temperature difference across
 274 the two ends of the thermocouple according to:

$$275 \quad \Delta T = T'_h - T'_c = \frac{T_h - T_c}{\left(1 + 2 \frac{\lambda \cdot h_p}{\lambda_p \cdot h_t} \right)} \quad (6)$$

276 where the effects related to the connected load should be considered. Really, if a resistive load
 277 is connected across the TE module terminals, an electrical current depending on the resistor
 278 value will flow in the load; low resistance values will produce an increment of the current and
 279 as a result the cooling of the hot junction and heating of the cold junction. The reduction of
 280 ΔT caused by this effect is dependent on the operating temperature and on the thermoelectric
 281 module properties and can be generally neglected.

282 Similarly, accounting for the electrical contact's contribution R_c , the total electrical resistance
 283 of TE module can be expressed as:

$$284 \quad R_{TE} = R + R_c = \frac{\rho \cdot h_t}{A_t} + 2 \frac{\rho_c}{A_t} = \frac{\rho(2 \cdot h_s + h_t)}{A_t} \quad (7)$$

285 being ρ_c the contact superficial resistivity and putting $h_s = \rho_c / \rho$. Combining (5), (6) and (7)
 286 a more accurate expression of thermal power extracted by a TE module is obtained:

$$287 \quad Q_{TE} = N_{TE} \left[\lambda \frac{A_t}{h_t} (T'_h - T'_c) + s \cdot T'_h \cdot I - \frac{1}{2} R_{TE} \cdot I^2 \right] \quad (8)$$

288 Considering m TE modules connected electrically in series and thermally in parallel, the
 289 expression:

$$290 \quad Q = m \cdot Q_{TE} \quad (9)$$

291 takes into account the heat flow passing through the thermocouple in steady state calculated
 292 as the sum of these three effects.

293 The first term in (8) accounts the heat conduction relevant to the temperature difference,
 294 the second one is the result of Peltier effects and the third term is representative of the Joule
 295 heating effect. Under these hypotheses, the current I , flowing in the electric load R_L connected
 296 to the TE generator, is given by:

$$297 \quad I = m \frac{V_{TE}}{R_{in} + R_L} = \frac{V_o}{R_{in} + R_L} \quad (10)$$

298 where R_{in} is the internal electrical resistance of the TE generator, given by

$$299 \quad R_{in} = m \cdot R_{TE} \quad (11)$$

$$300 \quad \text{and } V_o = m \cdot V_{TE} = m \cdot s \cdot N_{TE} (T'_h - T'_c) = m \cdot s \cdot N_{TE} \frac{(T_h - T_c)}{\left(1 + 2 \frac{\lambda \cdot h_p}{\lambda_p \cdot h_t}\right)} \quad (12)$$

301 the open-circuit voltage. The electric output power of the overall system is then [39]:

$$302 \quad P_{out_{TE}} = \frac{V_o^2 \cdot R_L}{(R_L + R_{in})^2} \quad (13)$$

303 and varies with R_L having a maximum when the load resistance match the internal resistance.
 304 Therefore, the load resistance value affects both the power generation performance and the
 305 Peltier effect at the interface with a change of temperature across the module. Particularly, in
 306 the case $R_L = R_{in}$ the maximum power transfer is realized with a negligible Peltier
 307 contribution to temperature reduction.

308 The electrical quantities in (10)-(13) are defined in terms of three materials properties
 309 (s, ρ, λ) that usually are not provided by manufacturers and vary with operating temperature.
 310 Generally, every manufacturer specifies the TE module producing performance curves,
 311 performance specifications $(Q_{TE_{max}}, I_{TE_{max}}, V_{TE_{max}}, \Delta T_{max}, R_{TE})$ and some geometrical parameters.
 312 The parameters (s, ρ, λ) can be accurately determined using experimental setup or using
 313 some theoretical equations [24], [40], [41]. Alternatively, these TE coefficients can be
 314 modelled, supposing a uniform temperature along the side of the module and using the
 315 operating temperature $T_m = (T_c + T_h)/2$ of the TE, by means of a second-order polynomials
 316 equation [42] depending on the manufacturer:

$$317 \quad \begin{aligned} s &= a(T_m - 23)^2 + b(T_m - 23) + c \\ \rho &= d(T_m - 23)^2 + e(T_m - 23) + f \\ \lambda &= g(T_m - 23)^2 + h(T_m - 23) + i \end{aligned} \quad (14)$$

$$318 \quad \begin{aligned} a &= -9.90 \cdot 10^{-10} [V/K^3]; b = 3.44 \cdot 10^{-7} [V/K^2]; c = 2.11 \cdot 10^{-4} [V/K]; \\ \text{with } d &= 6.28 \cdot 10^{-11} [\Omega \cdot mm/K^2]; e = 5.35 \cdot 10^{-8} [\Omega \cdot mm/K]; f = 10.85 \cdot 10^{-6} [\Omega \cdot mm]; \\ g &= 41.30 \cdot 10^{-6} [W / (mm \cdot K^3)]; h = -3.32 \cdot 10^{-3} [W / (mm \cdot K^2)]; i = 1.66 [W / (mm \cdot K)]; \end{aligned}$$

319 .

320 where the values used are related to CP2-127-06 TE module [43]. The consistence of the
 321 values obtained through (14) has been verified with Matlab simulations calculating the
 322 Seebeck coefficient s , the electrical resistivity ρ and the thermal conductance λ of the
 323 material on the basis the manufacturer's specifications $(Q_{TE_{max}}, I_{TE_{max}}, V_{TE_{max}}, \Delta T_{max}, R_{TE})$; to this
 324 aim, three TE modules have been considered, i.e. Tellurex C2-30-1503, Marlov RC-12-4 and

325 Kryotherm TB 127-1-1.0-1.3. They are designed for cooling and heating applications with
 326 geometrical, electrical and thermal parameters reported in TABLE III.

327 **TABLE III.** CHARACTERISTIC PARAMETERS OF THE CONSIDERED THERMOELECTRIC MODULES

Manufacturer	Model	Length [mm]	Width [mm]	Thickness [mm]	R_{TE} [Ω]	ΔT_{max} [K]	Q_{TEmax} [W]
Tellurex	C2-30-1503	30.00	30.00	3.70	3.85	341.15	34.1
Marlov	RC-12-4	29.97	29.97	3.43	3.20	339.15	36.0
Kryotherm	TB-127-1.0-1.3	30.00	30.00	3.60	3.20	342.15	34.5

328

329 In TABLE IV. the values of (s, ρ, λ) estimated for the three TE module are reported.

330 **TABLE IV.** s, ρ, λ OBTAINED BY FITTING MANUFACTURER'S SPECIFICATIONS

Manufacturer	Model	s [V/K]	ρ [Ω mm]	λ [W/mm K]
Tellurex	C2-30-1503	208.39e-6	10.07e-4	17.08e.3
Marlov	RC-12-4	209.24e-6	11.31e-4	16.07e.3
Kryotherm	TB-127-1.0-1.3	205.53e-6	10.06e-4	15.97e.3

331

332 The goodness of the model has been verified using the specifications of the CP2-127-06 TE
 333 module and comparing (see TABLE V.) the results of (14) with the results obtained by using
 334 the model in [44], [45] for different values of temperature; T_c values are the average
 335 temperatures relevant to both coldest and the hottest month of the year and T_h values are the
 336 front panel temperature evaluated through (1) considering the environmental parameters of
 337 the site (T_c, G) and PV panels installed on the top of roof with small roof-module distance
 338 ($c=0.036 K \cdot m^2/W$). An in-depth analysis of the results shows that the maximum deviation of
 339 the figure of merit $Z = s^2/\rho \lambda$ between estimated using (14) and [44], [45] is less than 0.7%.

340 **TABLE V.** COMPARISON BETWEEN s, ρ, λ ESTIMATION BY (14) AND [44], [45] USING THE CP2-127-08 TE
 341 SPECIFICATIONS

City	T_c [$^{\circ}$ C]	T_h [$^{\circ}$ C]	s [V/K]	ρ [Ω mm]	λ [W/mm K]	s [V/K]	ρ [Ω mm]	λ [W/mm K]
			Eq. (14)			[44], [45]		
Pachino (Sicily)	13	29	210.21e-6	10.74e-4	16.66e.3	210.26e-6	10.75e-4	16.66e.3
	28	48	215.84e-6	11.64e-4	16.18e.3	215.89e-6	11.67e-4	16.19e.3
Taranto	10	23	208.62e-6	10.50e-4	16.82e.3	208.67e-6	10.51e-4	16.83e.3
	27	46	215.37e-6	11.56e-4	16.22e.3	215.41e-6	11.59e-4	16.22e.3

Rome	9	21	208.08e-6	10.42e-4	16.88e.3	208.13e-6	10.43e-4	16.89e.3
	26	45	215.05e-6	11.51e-4	16.24e.3	215.09e-6	11.53e-4	16.25e.3
Turin	5	17	206.63e-6	10.20e-4	17.05e.3	206.68e-6	10.22e-4	17.05e.3
	25	41	214.25e-6	11.38e-4	16.30e.3	214.29e-6	11.40e-4	16.31e.3
Glasgow	5	9	205.14e-6	9.98e-4	17.23e.3	205.19e-6	10.02e-4	17.23e.3
	16	26	210.21e-6	10.74e-4	16.66e.3	210.26e-6	10.75e-4	16.66e.3
Stockholm	-1	3	202.85e-6	9.64e-4	17.52e.3	202.90e-6	9.71e-4	17.52e.3
	19	30	211.41e-6	10.93e-4	16.54e.3	211.46e-6	10.94e-4	16.55e.3

342

343

344 Finally, substituting in (10) - (13) the parameters s , ρ , \square estimated through (14) it is
345 possible to obtain the electrical parameters of the TE module.

346 D. PVTE PERFORMANCE INDEXES

347 The mathematical model of the hybrid system is based on the integration of the PV cells
348 with the TE modules previously described; the system combines radiation and thermal energy
349 to produce electricity. In particular, the PV cells convert solar radiation into electricity
350 whereas the TE modules transform the heat generated below the PV cells in electric power.

351 In this analysis it is assumed that the rear temperature of the panel almost equal to the
352 temperature present on the front side of the panel itself and that the TE module posteriorly
353 integrated into the PV panel with the hot junction at the same temperature of rear side of the
354 panel and the cold junction at ambient temperature [14], [46], [47].

355 It is well known that when the PV module works at the maximum power point, its output
356 power can be expressed as:

$$357 P_{out,max_{pv}} = I_{mp} \cdot V_{mp} \quad (15)$$

358 where I_{mp} and V_{mp} are the current and the voltage calculated at the maximum power point,
359 respectively, even if environmental conditions can produce performances variation especially
360 in PV plants where several modules are connected in string [48].

361 As regards the PV module, the efficiency assessed under the universally recognized
362 standard test conditions (STC), is expressed in terms of the open-circuit voltage and the short-
363 circuit current, as:

$$364 \varepsilon_{PV_{STC\%}} = \frac{FF \cdot I_{sc} \cdot V_{oc}}{A_p \cdot G_{STC}} \cdot 100 = \frac{I_{mp} \cdot V_{mp}}{A_p \cdot G_{STC}} \cdot 100 \quad (16)$$

365 where A_p and $FF = I_{mp} \cdot V_{mp} / I_{sc} \cdot V_{oc}$ are the area and fill factor of the PV panel, respectively.

366 Under these assumptions, the efficiency of the PV module at a generic radiance (G) is
367 expressed as:

$$368 \quad \varepsilon_{PV\%} = \frac{I_{mp} \cdot V_{mp}}{A_p \cdot G} \cdot 100 \quad (17)$$

369 while, the final yield, useful to compare different PV systems at the same operating site, is
370 expressed as:

$$371 \quad Y_{PV} = \frac{E_{PV}}{P_n} \quad (18)$$

372 where E_{PV} is the average energy that the PV panel generates monthly or yearly and P_n is the
373 nominal power of the solar generator. TE performance varies significantly with TE materials,
374 module geometry and contact properties; the maximum output power depends on both the
375 amount of input heat and of the load resistance R_L which should be as close as possible to the
376 internal electrical resistance of the thermo-generator R_{in} . Moreover the conversion efficiency
377 increases with temperature difference and thermo-element length [49]. In relation to R_{in} , the
378 power output of the TE module increases with the number of the modules because the electric
379 output power increases with “the square of m ” while efficiency remains almost unchanged.

380 It could occur that when the current in the thermo-element increases, the component
381 related to the Joule effect takes over on other energy components; this means a drastic
382 performance reduction in terms of both efficiency and power. For this reason, when the TE
383 module is forced to work under these conditions, it is preferred to increase m ; obviously, this
384 provides the physical limit for having no losses. However, where the space and the costs
385 allow it, the use of multiple TE modules is advisable to increase the output power.

386 Finally, the TE global efficiency and the final yield can be expressed as:

$$387 \quad \varepsilon_{TE} = \frac{P_{out_{TE}}}{Q} \quad (19)$$

388 In the proposed analysis $m=37$ TE modules integrated behind the PV panel have been
389 considered. In this case the total generated power of the PVTE hybrid system is the sum of the
390 power output of each system:

$$391 \quad P_{out,max_{PVTE}} = P_{out,max_{PV}} + P_{out_{TE}} \quad (20)$$

392 with a conversion efficiency given by:

$$\varepsilon_{PVTE\%} = \frac{P_{out,max_{PV}} + P_{out_{TE}}}{G} \cdot 100 \quad (21)$$

Then, the energy generated by the PVTE hybrid system is calculated by summing the overall power at each single hour as:

$$E_{PVTE} = P_{out,max_{PVTE}} \cdot h \quad (22)$$

where h represents the hours of average radiance; so the final yield of the overall system performance is:

$$Y_{PVTE} = \frac{E_{PVTE}}{P_n} \quad (23)$$

according to IEC standard 61724 [50].

III. TEST PERFORMANCE AND RESULTS

The performance of the PVTE system was characterized considering global radiation data at different sites by evaluating power and energy generated, efficiency and final yield for PV, TE and integrated PVTE system.

The sites have been chosen to verify how performance varies when the irradiance and the temperature distributions reach higher values. The radiance (G), the sunshine hours (d_h) and the ambient temperature (T_{amb}) used in the model have been obtained by using the online database provided by the Joint Research Centre of the European Commission and of the National Renewable Energy Laboratory [31].

In order to have a global view of the performance of the system under consideration, the data for each month of the year have been downloaded. For every day of each month the system acquires the data at regular intervals of 15 minutes sunrises to sunset; for each acquisition time the algorithm produces a mean of several measurements. TABLE VI. shows the average data of global radiance, ambient temperature and hours of daily radiance for best tilt solar panel. Data highlight that the towns closer to the equator have higher radiance and temperature values with respect to northern one with very similar trends. Small differences show Glasgow and Stockholm; in fact, during the coldest months of the year in Glasgow the radiance and the temperature are higher than in Stockholm while in the warmer months it is the opposite. Finally, the average hours of radiance over a year shows that in the winter months, the cities farthest from the equator have shorter days with respect to those in southern Europe; vice versa in the summer months, the cities in northern Europe have longer days and hence more hours of sunlight

423 In [38] an inclination angle of 0° was considered in order to verify the system performance
 424 with same initial conditions. Now, using best tilt angle, best performance should be estimated
 425 for each considered site.

426 **TABLE VI.** GLOBAL IRRADIANCE, AVERAGE TEMPERATURE AND DAYLIGHT HOURS FOR THE CONSIDERED SITES

Month	Stockholm			Glasgow			Turin			Rome			Taranto			Pachino (Sicily)		
	G [W/m ²]	T _{amb} [°C]	d _h [h]	G [W/m ²]	T _{amb} [°C]	d _h [h]	G [W/m ²]	T _{amb} [°C]	d _h [h]	G [W/m ²]	T _{amb} [°C]	d _h [h]	G [W/m ²]	T _{amb} [°C]	d _h [h]	G [W/m ²]	T _{amb} [°C]	d _h [h]
Jan	98	-1,1	06:15	121	4,9	07:15	325	5,2	08:45	330	9,2	09:15	360	10,3	09:15	433	12,7	09:45
Feb	194	-0,8	08:45	187	5,4	09:15	436	7,3	09:45	409	9,9	10:15	417	10,6	10:15	490	13,0	10:15
Mar	253	1,3	11:15	259	6,8	11:15	441	10,9	11:45	426	11,9	11:45	444	12,3	11:45	497	14,4	11:45
Apr	303	6,2	14:15	310	8,6	13:30	411	13,5	13:15	446	14,4	12:45	459	15,1	12:45	508	16,5	12:45
May	352	11,1	16:00	313	11,6	15:30	402	18,6	14:15	449	19,6	14:15	458	20,4	14:15	497	21,0	13:45
Jun	300	16,0	17:30	276	14,2	16:30	403	22,7	15:00	460	23,8	14:45	468	24,7	14:45	496	25,3	14:15
Jul	309	19,2	17:00	273	16,1	16:00	445	24,6	14:30	509	26,0	14:15	507	27,3	14:15	541	27,8	13:45
Aug	293	19,1	14:45	263	16,2	14:30	437	24,0	13:45	524	26,0	13:15	527	27,0	13:15	546	28,0	13:15
Sep	269	14,4	12:15	242	14,3	12:15	437	24,0	13:45	478	22,1	12:15	481	23,0	12:15	517	24,8	12:15
Oct	196	8,8	09:45	186	11,0	10:15	354	15,8	10:45	424	18,9	10:45	448	19,6	10:45	506	21,9	10:45
Nov	127	3,7	07:15	159	7,7	07:45	302	9,9	09:15	363	14,1	09:15	367	15,0	09:45	461	17,8	09:45
Dec	61	0,2	05:45	113	4,9	06:45	333	6,0	08:15	331	10,5	08:45	383	11,7	08:45	437	14,4	09:15
Best Tilt [°]	41			38			39			35			34			33		
Azimuth [°]	0			0			0			0			0			0		
Latitude	59°19'44" North			55°57'2" Nord			45°4'15" North			41°53'34" North			40°27'56" Nord			36°42'43" North		
Longitude	18°3'53" East			4°6'34" Ovest			7°41'8" East			12°28'57" East			17°14'52 Est			15°5'33" East		

427

428 The tests have been conducted according to the hypotheses of *i*) solar module subjected to
 429 uniform illumination without shadow zones, *ii*) equal rear and front panel temperature, *iii*) TE
 430 hot junction temperature equal to rear temperature of the PV, *iv*) TE cold junction temperature
 431 equal to the ambient temperature (by assuming that the system is not working with an
 432 additional cooling system). The PV panel front temperature is been calculated by equation (1)
 433 using the value $0.036 \text{ K}\cdot\text{m}^2/\text{W}$ for c and considering the monthly average data of temperature
 434 and global radiation for each location at different times of the day. It is worth to underline that
 435 there is a wide literature which analyses the correlation among temperature, weather
 436 conditions and material properties and then several models for cell temperature have been
 437 proposed as a function of the wind speed, solar radiation and ambient temperature in different
 438 implicit and explicit equations [52]. The performance of the method has also been verified
 439 using one PV panel and $m=37$ TE modules. The PV was a IP10P model by Istar Solar
 440 consisting of $N_p = 2$ parallel-connected strings each composed by $N_s=36$ series-connected
 441 polycrystalline silicon cells and provides a peak output of 10 W [53]; the dimensions of the

442 panel is 310 x 210 mm and its specifications in STC are listed in TABLE VII. The TE module
 443 considered was a TGM 127-1.0-1.3 [54] composed by 127 thermocouples connected
 444 thermally in parallel and electrically in series; the dimensions of the module is 30 x 30 mm;
 445 the thermal and electrical parameters of TE are presented in TABLE VIII. The TE generator
 446 was obtained considering thirty-seven TE modules connected electrically in series and
 447 thermally in parallel so to cover about 2/3 of the rear side of the cells.

448 **TABLE VII. IP10P SPECIFICATIONS IN STC**

<i>Symbol</i>	<i>Parameter</i>	<i>Value</i>
P_M	<i>Maximum Power (MP)</i>	10 W
V_{MP}	<i>Voltage @MP</i>	17 V
I_{MP}	<i>Current @MP</i>	0.6 A
V_{OC}	<i>Open-circuit Voltage</i>	21,6 V
I_{SC}	<i>Short-circuit Current</i>	0.67 A
α	<i>Current temperature coefficient</i>	0.07 %/°C
β	<i>Voltage temperature coefficient</i>	-0.34 %/°C

449

450 **TABLE VIII. TGM 127-1.0-1.3 PERFORMANCE**

<i>Symbol</i>	<i>Parameter</i>	<i>Value</i>
ΔT_{max}	<i>Maximum Temperature Difference</i>	150 °C
T_c	<i>Cold end Temperature</i>	0° C
V_{TE}	<i>Voltage</i>	2.5 V
I_{TE}	<i>Current</i>	0.59 A
P_{OUTTE}	<i>Power</i>	21,6 V

451

452 In TABLE IX. annual power and energy have been reported for each site; the values are been
 453 obtained summing the monthly values of power and energy. The TE module is more
 454 performing and helpful in warmer countries and the latitude mainly affects the performance of
 455 the TE generator with respect to PV panel; in fact, the value of E_{PV} is halved moving from
 456 Pachino to Glasgow or Stockholm, whereas the E_{TE} is reduced by about 1/3.

457

458

TABLE IX. ANNUAL POWER AND ENERGY CALCULATED FOR SITES CONSIDERED

	P_{PV} [W]	P_{TE} [W]	P_{PVTE} [W]	E_{PV} [Wh]	E_{TE} [Wh]	E_{PVTE} [Wh]
<i>Pachino (Sicily)</i>	1.737	239	1.976	20.198	2.792	22.989
<i>Taranto</i>	1.584	199	1.704	18.889	2.323	21.211
<i>Rome</i>	1.540	184	1.724	18.148	2.208	20.355
<i>Turin</i>	1.442	153	1.595	17.031	1.862	18.893
<i>Glasgow</i>	852	54	906	10.612	721	11.332
<i>Stockholm</i>	875	60	934	11.344	840	12.185

460

461 These conclusions seem to be confirmed considering the effect of the power and energy
462 produced by TE with respect to PVTE system where the TE module contributes to total
463 energy from 12.2 % in Pachino to about 6.5 % in Glasgow and Stockholm (TABLE X.). It is
464 worth to note that the TE generator sited in Stockholm, in a time frame of an year, has better
465 performance compared to the same TE generator in Glasgow despite Stockholm is more to
466 north of Glasgow. The final yield values reported in the same table, which represent the
467 annual produced energy normalised to rated power, are useful to compare the performance of
468 PVTE system for different configurations and sites. An in depth analysis of these data shows
469 that the final yield decrease no more than 45% for PV and up to 70% for TE. Same
470 performance can be achieved varying the number of thermo-modules. Other tests carried out
471 with the thermo-modules, and not reported in the paper for sake of brevity, seem to confirm
472 the exposed results.

473

TABLE X. FINAL YIELD, POWER AND ENERGY CALCULATED FOR THE CONSIDERED SITES

	P_{TE}/P_{PVTE}	E_{TE}/E_{PVTE}	Y_{FTE}	Y_{FPV}
<i>Pachino (Sicily)</i>	12,11	12,14	50,30	2016,84
<i>Taranto</i>	11,70	10,95	41,85	1864,30
<i>Rome</i>	10,65	10,85	39,78	1815,46
<i>Turin</i>	9,57	9,86	33,55	1702,95
<i>Glasgow</i>	5,98	6,36	12,99	1061,98
<i>Stockholm</i>	6,39	6,90	15,14	1133,83

474

475 Finally, in TABLE XI. the values of the relative deviation percentage between the PV
476 system and the hybrid system PVTE (d_{PVTE}) calculated for each month of the year, are
477 indicated.

478 The data highlight that d_{PVTE} ranges in the interval 7.78-16.08 for the cities of southern
479 Europe.

480

TABLE XI. PERCENTAGE PERFORMANCE " PVTE /PV" DEVIATION

Month	Pachino (Sicily)	Taranto	Rome	Turin	Glasgow	Stockholm
<i>Jan</i>	11,69	9,16	8,51	8,39	3,85	2,31
<i>Feb</i>	12,90	10,80	10,37	11,16	4,91	4,48
<i>Mar</i>	13,37	11,93	11,26	11,33	6,21	6,08
<i>Apr</i>	13,79	15,55	12,09	10,62	7,50	7,54
<i>May</i>	14,05	12,89	12,50	10,67	8,37	9,44
<i>Jun</i>	14,03	13,64	13,19	10,98	7,05	8,22
<i>Jul</i>	15,70	14,48	14,82	12,51	7,23	8,17
<i>Aug</i>	16,08	14,97	14,93	12,06	6,59	7,76
<i>Sep</i>	15,03	13,61	13,64	12,06	6,07	7,25
<i>Oct</i>	13,90	12,50	11,35	9,73	5,17	4,79
<i>Nov</i>	12,55	10,00	9,41	7,78	4,43	3,63
<i>Dec</i>	11,75	9,92	8,55	8,22	4,18	0,98

482

483 The best performances are obtained in August in the Pachino city (green cell) even if the
484 TE power contribution is considerable in each site in the spring and summer months. Lower
485 performance are obtained in northern towns (Glasgow and Stockholm), especially in the
486 winter months; this unfavourable phenomenon happens in the particularly cold months of
487 January and December in the city of Stockholm (red cells). In the same table, cells in yellow
488 highlight that the maximum values are obtained, in all the cities, in the month of July or
489 August except in Glasgow and Stockholm in which they are obtained in May. Although the
490 TE module enhances annual PV performance, the extra cost of this device should be balanced
491 by the energy produced. TE devices price varies from manufactures to manufacturer and TE
492 materials keeps changing on with changing times. So, new products to the market bring
493 fluctuation in TE price. Commercial modules are available in many size and with different
494 power; generally, the price reduces when the power increases and for large quantities.
495 Typical costs for TE generating modules varies from 2.40 to 6.80 \$/W, which is higher than
496 normal solar price of 0.58-1.28 \$/W [55]; so the global extra cost of about four-five times
497 higher than PV module makes less attractive current TE technology for this application and
498 requires new researches in order to increase the efficiency and reduce the cost of these
499 devices. However, the results suggest that to obtain systems with good reliability and cost-
500 effective the design of a PVTE system should be tailored to location, individual requirements
501 and meteorological condition and that the optimal number of TE module is dependent on the
502 resistance of PV panel, on the type of components used and on the environmental parameters
503 of the site.

504

505

IV. CONCLUSIONS

506 In the paper a complete model to evaluate the performance of a PVTE hybrid system is
507 proposed and verified by simulation results. The obtained results seem to shown that the PV
508 module is the primary source of energy of the system, even if the TE contribution is
509 significant in southern Europe towns and that best performance are obtained for the locations
510 having high radiance and low ambient temperature. A detailed analysis of the results indicated
511 that the TE module produce good performance in the spring and summer months assuring
512 promising contribution of energy even if the load resistance, the meteorological conditions
513 and site should be carefully considered. New further research in TE material seem to promise
514 high values of the figure of merit Z so to increase the TE efficiency up to 50%.; under this
515 assumption the TE technology would be a viable candidate for alternative power generation.

516

517 ACKNOWLEDGMENT

518 The authors would like to thank Eng. D. Passaghe for his valuable contribution.

519

REFERENCES

- 520 [1] A. Malik, E. Grohmann, Environmental Protection Strategies for Sustainable Development, Springer, 2012.
- 521 [2] B. Sørensen, Renewable Energy: Its Physics, Engineering, Use, Environmental Impacts, Economy, and
522 Planning Aspect, Academic Press, 2011.
- 523 [3] V. V. Tyagi, N. A. A. Rahim, N. A. Rahim, J. A. L.Selvaraj, Progress in solar PV technology: Research
524 and achievement, Renewable and Sustainable Energy Reviews, n. 20 , April 2013, pp. 443-461.
- 525 [4] B. Parida, S. Iniyani, Ranko Goic, A review of solar photovoltaic technologies, Renewable and Sustainable
526 Energy Reviews n.15, April 2011, pp. 1625 -1636.
- 527 [5] A. Gaur, G.N. Tiwari, Performance of a-Si thin film PV modules with and without water flow: An
528 experimental validation, Applied Energy, vol. 128, no. 1, September 2014, pp. 184-191.
- 529 [6] A. Carullo, S. Corbellini, A. Luoni, A. Neri, In situ calibration of heterogeneous acquisition systems:
530 the monitoring system of a photovoltaic plant, IEEE Transactions on Instrument and Measurement, vol.
531 59, no. 5, April 2010, pp. 1098-1103.
- 532 [7] L. Cristaldi, M. Faifer, M. Rossi, S. Toscani, An Improved Model-Based Maximum Power Point
533 Tracker for Photovoltaic Panels, IEEE Transactions on Instrument and Measurement, vol. 63, no. 1,
534 January 2014, pp. 63-71.
- 535 [8] A. Luque, S. Hegedus, Handbook of Photovoltaic Science and Engineering, Wiley, 2003.
- 536 [9] M. M. M. Daud, N. B. M. Nor, T. Ibrahim, Novel Hybrid Photovoltaic and Thermoelectric Panel, Proc. of
537 International Power Engineering and Optimization Conference, Melaka, Malaysia, June 2012, pp. 269-274.

- 538 [10]M. Fuentes, G. Nonfuentes, J. Aguilera, D. L. Talavera, M. Castro, Application and Validation of Algebraic
539 Methods to Predict the Behaviour of Crystalline Silicon PV Modules in Mediterranean Climates, *Solar*
540 *Energy*, vol. 81, November 2007, pp. 1396-1408.
- 541 [11]W. G. J. H. M. Van Sark, Feasibility of Photovoltaic-Thermoelectric hybrid Modules, *Applied Energy*, vol.
542 88, August 2011, pp. 2785-2790.
- 543 [12]H. Sasaki, K. Takahashi, D. Inglis, M. Klons, A numerical Simulation of Thermoelectric Effects in Single-
544 Junction Thermal Converters, *IEEE Transactions on Instrumentation and Measurement*, vol.48, no. 2, April
545 1999, pp. 408-411.
- 546 [13]S. Dalola, M. Ferrari, V. Ferrari, M. Guizzetti, D. Marioli, A. Taroni, Characterization of Thermoelectric
547 Modules for Powering Autonomous Sensors, *IEEE Trans. on Instrumentation and Measurement*, vol. 58, April
548 2009, pp. 99-107.
- 549 [14]D. Yang, H. Yin, Energy Conversion Efficiency of a Novel Hybrid Solar System for Photovoltaic,
550 Thermoelectric and Heat Utilization, *IEEE Transaction on Energy Conversion*, vol. 26, September 2011, pp.
551 662-670.
- 552 [15]S. Dalola, V. Ferrari, M. Guizzetti, D. Marioli, E. Sardini, M. Serpelloni, A. Taroni, Autonomous Sensor
553 System with Power Harvesting for Telemetric Temperature Measurements of Pipes, *IEEE Transactions on*
554 *Instrumentation and Measurement*, vol.58, no. 5, May 2009, pp.1 471-1478.
- 555 [16]M. Chen, Distributed Detection and Control of Defective Thermoelectric Generation Modules Using Sensor
556 Nodes, *IEEE Transactions on Instrumentation and Measurement*, vol.63, no. 1, January 2014, pp.192-202.
- 557 [17]W. He, J. Zhou, C. Chen, J. Ji, Experimental study and performance analysis of a thermoelectric cooling and
558 heating system driven by a photovoltaic/thermal system in summer and winter operation modes, *Energy*
559 *Conversion and Management*, n. 84, August 2014, pp. 41-49.
- 560 [18] M. Herrando, C. N. Markides, K. Hellgardt, A UK-based assessment of hybrid PV and solar-thermal
561 systems for domestic heating and power: System performance, *Applied Energy*, n. 122, June 2014, pp 288-
562 309 .
- 563 [19]J.- A. Jiang, Y. L. Su, J. C. Shieh, K. C. Kuo, T. S. L. T. T. Lin, W. Fang, J. J. Chou, J. C. Wang, On
564 application of a new hybrid maximum power point tracking (MPPT) based photovoltaic system to the closed
565 plant factory, *Applied Energy*, n. 124, n. 1, July 2014, pp. 309-324.
- 566 [20]D. Kamthania, G.N. Tiwari, Energy metrics analysis of semi-transparent hybrid PVT double pass facade
567 considering various silicon and non-silicon based PV module *Hyphen Solar Energy*, n. 100, February 2014,
568 pp. 124-140.
- 569 [21]H. Chen, N. Wang, H. He, Equivalent Circuit Analysis of Photovoltaic-Thermoelectric Hybrid Device with
570 Different TE Module Structure, *Advances in Condensed Matter Physics*, n. 2014, May 2014, pp. 1-6.
- 571 [22]G. Andria, A M.L. Lanzolla, F. Piccininni, G. S. Virk , Design and Characterization of Solar Assisted
572 Heating Plant in Domestic Houses, *IEEE Transactions on Instrumentation and Measurement*, vol. 57, no. 12,
573 December 2008, pp. 2711-2719.
- 574 [23]H. A. Zondag, Flat-plate PV-Thermal Collectors and Systems: a Review, *Renewable Sustainable Energy*,
575 vol. 12, May 2008, pp. 1-16.

- 576 [24]D. Mitrani, J. A. Tomé, J. Salazar, A. Turò, Methodology for Extracting Thermoelectric Module Parameters,
577 vol. 54, August 2005, pp. 1548-1552.
- 578 [25]W. G. J. H. M. van Sark, Feasibility of Photovoltaic - Thermoelectric hybrid Modules, Applied Energy, vol.
579 88, August 2011, pp. 2785-2790.
- 580 [26] S. LeBlanc, S. K. Yee, M. L. Scullin, C. Damesd, K. E. Goodson, Material and manufacturing cost
581 considerations for thermoelectrics, Renewable and Sustainable Energy Reviews, n. 32 , April 2014,
582 pp.313–327.
- 583 [27]X. Zhang, K. T. Chau, C. C. Chan, S. Gao, An Automotive Thermoelectric-Photovoltaic Hybrid Energy
584 System, Proc. of IEEE Vehicle Power and Propulsion Conference, Lille, France, September, 2010, pp. 1-5.
- 585 [28]W. Roth, R. Kugele, A. Steinhoser, W. Schulz, G. Hille, Grid-independent power supply for repeaters in
586 mobile radio networks using photovoltaic-thermoelectric hybrid systems, Proc. of Thermoelectrics
587 International Conference, Cardiff, Wales, September 1997, pp. 582-585.
- 588 [29]N. Smith, R. Mc Cann, Investigation of a Multiple Input Converter for Grid Connected Thermoelectric-
589 Photovoltaic Hybrid System, Proc. of IEEE Green Technologies Conference, Tulsa, USA, April 2012, pp. 1-
590 5.
- 591 [30]Y. Fan, L. Ge, W. Hua, Multiple-input DC-DC Converter for the Thermoelectric-Photovoltaic Energy
592 System, Proc. of IEEE Vehicle Power and Propulsion Conference, Lille, France, September, 2010, pp. 6-10.
- 593 [31]Photovoltaic Geographical Information System (PVGIS), <http://re.jrc.ec.europa.eu/pvgis/>
- 594 [32]A. Drews, A. C. de Keizer, H. G. Beyer, Monitoring and Remote Failure Detection of Grid-Connected, Solar
595 Energy, vol. 81, September 2007, pp. 548-564.
- 596 [33]M. R. Al Rashidi, M. F. Al Hajri, K. M. El-Naggar, A. K. Al-Othman, A New Estimation Approach for
597 Determining the I–V Characteristics of Solar Cells, Solar Energy, July 2011, vol. 85, pp. 1543-1550.
- 598 [34]A. Goetzberger, V. U. Hoffmann, Photovoltaic Solar Energy Generation, Spingler-Verlag, 2005.
- 599 [35]F. Adamo, F. Attivissimo, A. Di Nisio, M. Spadavecchia, Characterization and Testing of a Tool for
600 Photovoltaic Panel Modeling, IEEE Trans. on Instrum. Meas., April 2011, vol. 60, pp. 1613-1622.
- 601 [36]F. Attivissimo, A. Di Nisio, M. Savino, M. Spadavecchia, Uncertainty analysis in photovoltaic cell
602 parameters estimation, IEEE Trans. on Instrum. Meas., April 2012, vol. 61, pp. 1334-1342.
- 603 [37]F. Adamo, F. Attivissimo, A. Carullo, A. M. L. Lanzolla, F. Spertino, A. Vallan, On the Performance of the
604 Double-diode Model in Estimating the Maximum Power Point for Different Photovoltaic Technologies,
605 Measurement, June 2013, vol. 46, pp. 3549-3559.
- 606 [38]F. Attivissimo, D. Passaghe, A. M. L. Lanzolla, M. Paul, D. Gregory, A. Knox, Photovoltaic-Thermoelectric
607 modules: a feasibility study, Proc.of I2MTC/14, Montevideo, Uruguay, May 2014, pp. 659-664.
- 608 [39]J. Gao, M. Chen, Beat the Deviation in Estimating Maximum Power of Thermoelectric Modules, IEEE
609 Transactions on Instrumentation and Measurement, vol. 62, no. 10, October 2013, pp. 2725-2729.
- 610 [40]D. Rowe, CRC Handbook of Thermoelectrics, CRC , 1995.
- 611 [41]J. L. Bierscheck, D. A. Johson, Latest Developments in Thermoelectrically Enhanced Heat Sink, August
612 2005, vol. 11, pp. 659-664.

- 613 [42]G. Casano, S. Piva, Experimental Investigation of the Performance of a Thermoelectric Generator based on
614 Peltier Cells, October 2011, vol. 35, pp. 660-669.
- 615 [43]https://home.zhaw.ch/~fusa/PSS_VLE_C/CHAPTER_03/CASES/Materials/CP2-127-06L.pdf
- 616 [44]N. Le Pierres, M. Cosnier, L. Luo, G. Fraisse, Coupling of Thermoelectric modules with a Photovoltaic Panel
617 for Air Preheating and precooling application: an annual simulation, Journal of Energy Research, July 2008,
618 vol. 32, pp. 1316-1328.
- 619 [45]S. B. Riffat, X. Ma, R. Wilson, Performance Simulation and Experimental Testing of a Novel Thermoelectric
620 Heat Pump System, Applied Thermal Engineering, October 2006, vol. 26, pp. 494-501.
- 621 [46]N. Wang, L. Han, H. He, N. H. Park, K. Koumoto, A Novel High-performance Photovoltaic-thermoelectric
622 Hybrid Device, Energy and Environmental Science, vol. 9, no. 4, August 2011, pp. 3676-3679.
- 623 [47]E. A. Chavez-Urbiola, Y. V. Vorobiev, L. P. Bulat, Solar Hybrid Systems with Thermoelectric Generators,
624 Solar Energy, vol. 86, September 2012, pp. 369-378.
- 625 [48]L. Cristaldi, M. Faifer, M. Rossi, S. Toscani, An Improved Model-Based Maximum Power Point Tracker for
626 Photovoltaic Panels, IEEE Trans. on Instrum. Meas., January 2014, vol 63, pp. 63-71.
- 627 [49]D. M. Rowe, G. Min, Evaluation of Thermoelectric Modules for Power Generation, Journal of Power
628 Sources, June 1998, vol. 73, pp. 193-198.
- 629 [50]IEC, Photovoltaic System Performance Monitoring - Guidelines for Measurement, data exchange and
630 Analysis, IEC Standard 61724, Geneva, Switzerland, 1998.
- 631 [51]National Renewable Energy Laboratory (SOLPOS), <http://www.nrel.gov/midc/>
- 632 [52]E. Skoplaki, J. A. Palyvos, Operating Temperature of photovoltaic modules: A survey of pertinent
633 correlations, Renewable Energy, June 2009, vol. 34, pp. 23-29.
- 634 [53]www.istarsolar.com/upload/imagefile/pdf/moduli/poly/is10P-is20P-is30P-is45P-is50P_IT_513.pdf
- 635 [54]www.eureca.de/english/cooling_teg_kryotherm.html
- 636 [55]www.ecobusinesslinks.com/surveys/free-solar-panel-price-survey